Results in Physics 7 (2017) 2085–2095

Contents lists available at ScienceDirect

Results in Physics

journal homepage: www.journals.elsevier.com/results-in-physics

Evaluation of the brightness of lightning channels and branches using the magnitude system: Application of astronomical photometry

Nobuaki Shimoji [a,*], Shouta Kuninaka [b,1], Kana Izumi [b]

[a] Department of Electrical and Systems Engineering, University of the Ryukyus, 1 Senbaru, Nishihara, Okinawa, 903-0213, Japan
[b] Department of Electrical and Electronics Engineering, University of the Ryukyus, 1 Senbaru, Nishihara, Okinawa, 903-0213, Japan

ARTICLE INFO

Article history:
Received 3 February 2017
Received in revised form 10 June 2017
Accepted 11 June 2017
Available online 21 June 2017

Keywords:
Lightning
Fechner's law
Magnitude system
Astronomical photometry
Image analysis

ABSTRACT

In this paper, we have evaluated the brightness of lightning leaders shown in a digital still image by applying the astronomical magnitude system. In order to analyze the only lightning leaders, these were extracted from the digital still image. For photometry of the lightning leaders, there is no a standard reference source such as Vega in astronomical photometry. Therefore, assuming the maximum pixel value 255 (in 256 levels) as the brightness of a standard reference source, the magnitude of the lightning leaders was obtained. The result showed that the magnitude of the lightning leaders vary spatially (i.e. 2D spatial variability). Furthermore, the result suggested that a low current channel is high magnitude and a high current channel is low magnitude.

Introduction

It is considered that the light emitted from a lightning leaders contains information in the lightning leaders. For example, it has been reported that there is a correlation between channel brightness and channel currents [1–6]. However, the study to classify lightning leaders by evaluating its brightness have not been reported so far. We consider that classifying the channel brightness may be utilized as a new method to analyze the lightning leaders.

In astronomy, since the surface of a star is Planckian radiator and color of the star is related to its surface temperature, there are many studies for the brightness and color of stars. The brightness of a star is classified by a magnitude system. For example, the Sun has a magnitude of −26.7, the full moon is −12.7 and Venus is −4.7 [7].

In what follows, the historical development of astronomical photometry is briefly explained. In the second century BCE, the ancient Greek astronomer Hipparchus divided stars visible with naked-eye into six magnitudes; and he compiled a star catalogue [8]. He defined the magnitude of brightest stars as first magnitude and that of the faintest stars as sixth magnitude. An ancient astronomer Claudius Ptolemy (about 90–168 CE) compiled the Almagest in which the magnitude scale by Hipparchus have been used [8]. It has then been found by Sir John Herschel (1792–1871) that a star of first magnitude is 100 times more brighter than that of sixth magnitude (for example, see Refs. [9,10]). This fact was defined by comparing the brightness of stars that was observed varying the aperture of the mirror of a telescope (well summarized in Ref. [10]). Norman Robert Pogson (1829–1891) formalized the magnitude system above. The equation by N. R. Pogson is given by [11]

$$\frac{B_i}{B_j} = 100^{(m_j - m_i)/5}, \tag{1}$$

where B_i and B_j are the brightness of i and jth stars and m_i and m_j are the magnitude of i and jth stars. Eq. (1) suggests that a star of nth magnitude is 2.512 ($\simeq 100^{1/5}$) times brighter than that of $(n+1)$th magnitude. The factor 2.512 is known as Pogson's ratio [10]. Taking the common logarithm of both sides in Eq. (1), the equation can be expressed by $m_i - m_j = -2.5\log_{10} B_i/B_j$, and it is called the Pogson's equation [11]. The Pogson's equation agree with the Fechner's law which states that the human perception is proportional to the logarithm of the physical stimulus [10,12]. That is, it is found that the magnitude system in astronomical photometry is based on the sensitivity of the human naked-eye.

As with the astronomical magnitude system, quantitative evaluation of the brightness of lightning leaders will be possible on the basis of the human naked eye. Although lightning channels are to be optically thin [13,14] it is meaningful to quantitatively investigate the brightness of lightning channel. It is known that a

* Corresponding author.
E-mail address: nshimoji@tec.u-ryukyu.ac.jp (N. Shimoji).
[1] Present address: Naha Data Center Co., Ltd., Japan.

http://dx.doi.org/10.1016/j.rinp.2017.06.013
2211-3797/

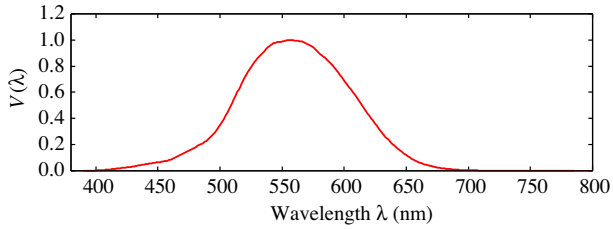

Fig. 1. Standard luminous efficiency function $V(\lambda)$ for photopic vision of the human eye (downloaded at http://www.cvrl.org/, last accessed on October 26, 2016).

grayscale digital image is based on the tristimulus value Y of the CIE XYZ color space, and Y is also based on the standard luminous efficiency function $V(\lambda)$ for photopic vision [15] ($V(\lambda)$ is shown in Fig. 1). Therefore, using the grayscale digital image, brightness evaluation based on the human naked eye is possible.

The purpose of this study is to quantitatively evaluate the brightness of lightning channel. In order to evaluate the brightness of lightning leaders, we have applied the magnitude system in astronomical photometry. Evaluating the only lightning leaders shown in a digital still image, we extracted the lightning leaders from the digital still image using the OpenCV library[2]; and then using the image showing the extracted leaders, the magnitude of the lightning channels was calculated. The obtained result suggested that the channel magnitude vary spatially.

Theoretical background

In the current era, using the fluxes F_i and F_j, (in watts per square meter, W·m^{-2}) of i and jth stars, the Pogson's equation is expressed as $m_i - m_j = -2.5\log_{10}F_i/F_j$, where m_i and m_j are the apparent magnitudes of the i and jth stars. Choosing a standard reference star such as Alpha Lyra (Vega), the apparent magnitude m of a star is given by $m - m_0 = -2.5\log_{10}F/F_0$, where F and F_0 are the fluxes of the star and the standard reference star, respectively; and thus since $m_0 = 0$, the magnitude of the star is given by $m = -2.5\log_{10}F/F_0$. In Vega magnitude system, the apparent magnitude m of a star is given by $m - m_0 = -2.5\log_{10}F/F_0$, where F and F_0 are the fluxes of the star and the standard reference star, respectively; and thus the magnitude of the star is given by $m = -2.5\log_{10}F/F_0$ since $m_0 = 0$. (Strictly speaking, Vega is the 0.03 magnitude star.)

It is well known that the brightness in a grayscale image is equal to the tristimulus value Y of the CIE XYZ color space. The tristimulus value Y on one pixel can also be considered as the illuminance in the unit lux (lx), which is equal to lumens per square meter, lm·m^{-2}. Usually a digital color image made with a digital still camera consists of R, G and B components. The illuminance Y can be written as [15–17]:

$$Y = 0.2126R + 0.7152G + 0.0722B,$$

where R, G and B are the pixel values (in 256 levels) of the R, G and B components in a digital color image. The illuminance Y is also given by [15,18]

$$Y = K_{\mathrm{m}} \int_{-\infty}^{\infty} \Phi_{\mathrm{e},\lambda}\, \bar{y}(\lambda) d\lambda, \tag{2}$$

where K_{m} is the maximum luminous efficiency 683 lm · W^{-1}, $\Phi_{\mathrm{e},\lambda}$ is the spectral radiant flux W·nm^{-1}, and $\bar{y}(\lambda)$ is the color-matching function, which is dimensionless. The color-matching function $\bar{y}(\lambda)$ is identical to the standard luminous efficiency function $V(\lambda)$ (shown in Fig. 1) for photopic vision. Therefore, it is found that the grayscale image is closely related to the sensitivity of photopic vision of the human naked eye. Moreover, it is found that taking the common logarithm of the illuminance Y equal to the brightness of the grayscale image is correspond closely to the Fechner's law; therefore, in the same way as astronomical photometry, the brightness of lightning branches and channels can be evaluated on the basis of the human naked eye.

The tristimulus value Y_i on an ith pixel is expressed as

$$\begin{aligned} Y_i =& K_{\mathrm{m}} \int_{-\infty}^{\infty} \frac{\Phi_{\mathrm{e},\lambda}^{\mathrm{ith}}}{S}\, \bar{y}(\lambda)\, d\lambda, \\ =& K_{\mathrm{m}} \int_{-\infty}^{\infty} E_{\mathrm{e},\lambda}^{\mathrm{ith}}\, \bar{y}(\lambda)\, d\lambda, \end{aligned} \tag{3}$$

where $\Phi_{\mathrm{e},\lambda}^{\mathrm{ith}}$ is the spectral radiant flux on an ith pixel in W·nm^{-1}, S is the photo-active area on each pixel in m^2, $E_{\mathrm{e},\lambda}^{\mathrm{ith}}$ is the spectral irradiance on an ith pixel in W · m^{-2} · nm^{-1} and Y_i is in lumens per square meter (lm·m^{-2}). From the unit lm·m^{-2} of Y_i, the tristimulus value Y_i on the ith pixel can be considered as the illuminance in lx (= lm · m^{-2}) on the ith pixel. In color science such as colorimetry and traditional photometry and radiometry, the radiant flux per square meter per wavelength is called the spectral irradiance W · m^{-2} · nm^{-1} and usually denoted by $E_{\mathrm{e},\lambda}$; whereas in astronomical photometry it is called the flux density W · m^{-2} · nm^{-1} and denoted by F_λ. In other words, the spectral irradiance in color science is equal to the flux density in astronomical photometry, i.e. $E_{\mathrm{e},\lambda} = F_\lambda$. To prevent confusion with the technical terms, in the following, we use the terms "flux density" F_λ W · m^{-2} · nm^{-1} for the radiant flux per square meter per wavelength. Thus Y_i (Eq. (3)) can be written as

$$Y_i = K_{\mathrm{m}} \int_{-\infty}^{\infty} F_{i,\lambda}\, \bar{y}(\lambda)\, d\lambda.$$

In this study, we have used the digital still image shot by setting the camera to bulb mode (exposure duration: $t_1 - t_0$); and thus the brightness per pixel is the time-integrated illuminance Y'. The time-integrated illuminance Y'_i in lm·s is given by

$$\begin{aligned} Y'_i =& \int_{t_0}^{t_1} dt\; Y_i = \int_{t_0}^{t_1} dt \left(K_{\mathrm{m}} \int_{-\infty}^{\infty} d\lambda\; F_{\lambda,i}(t)\; \bar{y}(\lambda) \right) \\ =& K_{\mathrm{m}} \int_{-\infty}^{\infty} d\lambda\; \bar{y}(\lambda) \int_{t_0}^{t_1} dt\; F_{\lambda,i}(t) \\ =& K_{\mathrm{m}} \int_{-\infty}^{\infty} d\lambda\; \bar{y}(\lambda)\; F'_{\lambda,i} \\ =& K_{\mathrm{m}} F'_i, \end{aligned}$$

where t_0 and t_1 are the beginning and end of exposure, $F'_{\lambda,i} = \int_{t_0}^{t_1} dt F_{\lambda,i}(t)$ is the time-integrated flux density W · m^{-2} · nm^{-1} · s and $F'_i = \int_{-\infty}^{\infty} d\lambda \bar{y}(\lambda) F'_{\lambda,i}$ is the time-integrated flux W · m^{-2} · s.

Moreover, Y'_i divided by the exposure duration $t_1 - t_0$, i.e. $Y'_i/(t_1 - t_0)$, is equal to the illuminance in lm·m^{-2} on ith pixel. The fraction of the illuminance $Y'_i/(t_1 - t_0)$ on ith pixel and $Y'_j/(t_1 - t_0)$ on jth pixel can be written as

$$\frac{Y'_i/(t_1 - t_0)}{Y'_j/(t_1 - t_0)} = \frac{Y'_i}{Y'_j} = \frac{K_m F'_i}{K_m F'_j} = \frac{F'_i}{F'_j} = \frac{F'_i/(t_1 - t_0)}{F'_j/(t_1 - t_0)}.$$

That is, the fraction of the fluxes $F'_i/(t_1 - t_0)$ and $F'_j/(t_1 - t_0)$ in W · m^{-2} can be expressed as the fraction of the time-integrated illuminance Y'_i and Y'_j on respective i and jth pixels; therefore applying the Pogson's equation to the i and jth pixels, the difference of the magnitudes, m_i and m_j, of the i and jth pixels can be expressed by

[2] OpenCV (Open Source Computer Vision Library) version 3.1.0, (released on December 21, 2015, downloaded on July 21, 2016).

$$m_i - m_j = -2.5\log_{10}\frac{F_i'/(t_1-t_0)}{F_j'/(t_1-t_0)} = -2.5\log_{10}\frac{Y_i'}{Y_j'}. \quad (4)$$

Material and calculation method

Lightning image

Fig. 2 shows the lightning flash image used in this work, that was captured in Chikusei City, Ibaraki Prefecture, Japan, on October 27th, 2008. Shooting location of the image is latitude: 36.284516°N and longitude 139.9638°E, where the location is defined in the World Geodetic System 1984 (WGS84). The camera used is a digital still camera (Canon EOS KISS Digital X) with a lens (TAMRON AF28–300 mm F/3.5–6.3 XR Di LD Aspherical [IF] MACRO (Model A061)). The specification of the camera is described in Appendix A. When the image was captured, optical filters such as ND filter and color filter were not used; furthermore the image was saved as RAW image data. The RAW image data is unprocessed signal data obtained from the image sensor of the digital still camera. Then the RAW image was imported to the RAW development software, Silkypix Developer Studio Pro.7 (Ichikawa Soft Laboratory, Co., Ltd.); and an uncompressed 16 bit image that is a tagged image file format (TIFF) image was generated. The image has the following properties: image size: 3000 × 2000 pixels, color space: sRGB, date: October 27, 2008, beginning time: 21:31:33 JST (12:31:33 UTC), exposure duration: 36 s, where JST means Japan Standard Time and it is given by JST = UTC(Coordinated Universal Time) + 9 h.

In Fig. 2, it is found that the right-side strike channel emerges from the emerging position; the primary branch leader channel is originated from the right-side strike channel; the left-side strike channel and other branch leaders are originated from the primary branch leader; and the three branches located in the right side of the right-side strike channel emerge from the cloud base. According to lightning data[3] obtained by the Japan Lightning Detection Network (JLDN),[4] the estimated peak currents I_{left} and I_{right} of the left- and right-side strike channels are $I_{left} = 11$ kA and $I_{right} = 35$ kA (see Appendix B).

Pretreatment

Extraction of lightning channel. In the lightning flash image (Fig. 2), there are many unwanted objects such as cloud luminescence, artificial light, and buildings. In order to analyze the only lightning leaders in Fig. 2, we have extracted these leaders by applying image processing techniques[5] and the extraction method is explained in the Appendix C.

Conversion to a grayscale image. Calculating magnitude of lightning channel, we have converted the color image showing the extracted image to a grayscale image. In this work we used the function "cv::imread" in OpenCV library; and the flag parameter was set to "CV_LOAD_IMAGE_GRAYSCALE".

Calculation of magnitude of lightning leaders

Using the grayscale pixel value, magnitude of the lightning channel was calculated. In astronomical photometry, there are standard reference sources such as Alpha Lyra (Vega); however there is no a standard reference source for the photometry to investigate lightning leaders. Therefore, in this work, we assumed the brightest value 255 (in 256 levels) in the grayscale image as the standard reference brightness for calculation of magnitude.

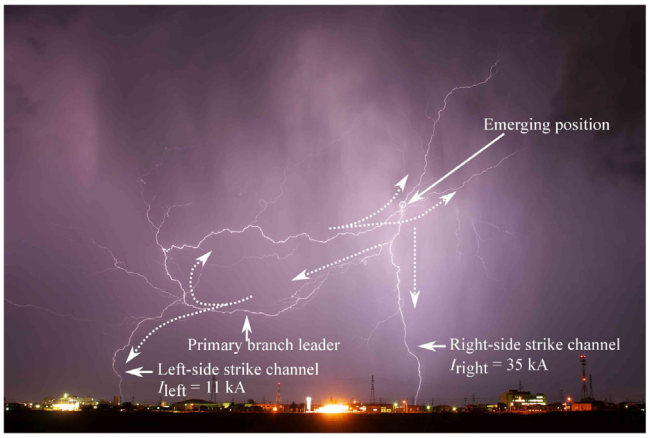

Fig. 2. Lightning flash image (Image courtesy of Mr. Yutaka Aoki). It can be seen that the lightning flash consists of the right-side strike channel ($I_{right} = 35$ kA), the primary branch leader originated from the right-side strike channel, the left-side strike channel ($I_{left} = 11$ kA) and other branch leaders originated from the primary branch leader. The dotted arrows indicate the direction of leader propagation.

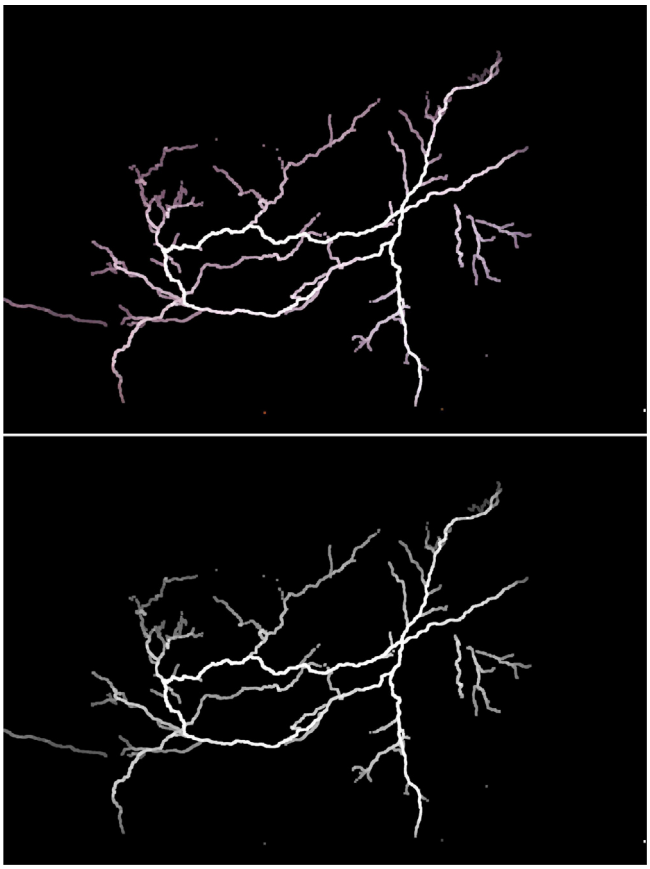

Fig. 3. (Upper) Extracted lightning channels and branches obtained by applying the image processing techniques explained in Appendix C and (Lower) grayscale image converted from the color image showing the extracted lightning channels and branches. The both (Upper) and (Lower) images have 256 levels and these are thickened using the function "cvDilate" in OpenCV library (parameter: "iterations" = 5) to improve visibility since these are very thin and less-visible. (For interpretation of the references to colour in this figure legend, the reader is referred to the web version of this article.)

[3] The lightning data was provided by Franklin Japan Corporation.
[4] The JLDN is maintained by Franklin Japan Corporation.
[5] In this study, image processing was performed by using the OpenCV library [19].

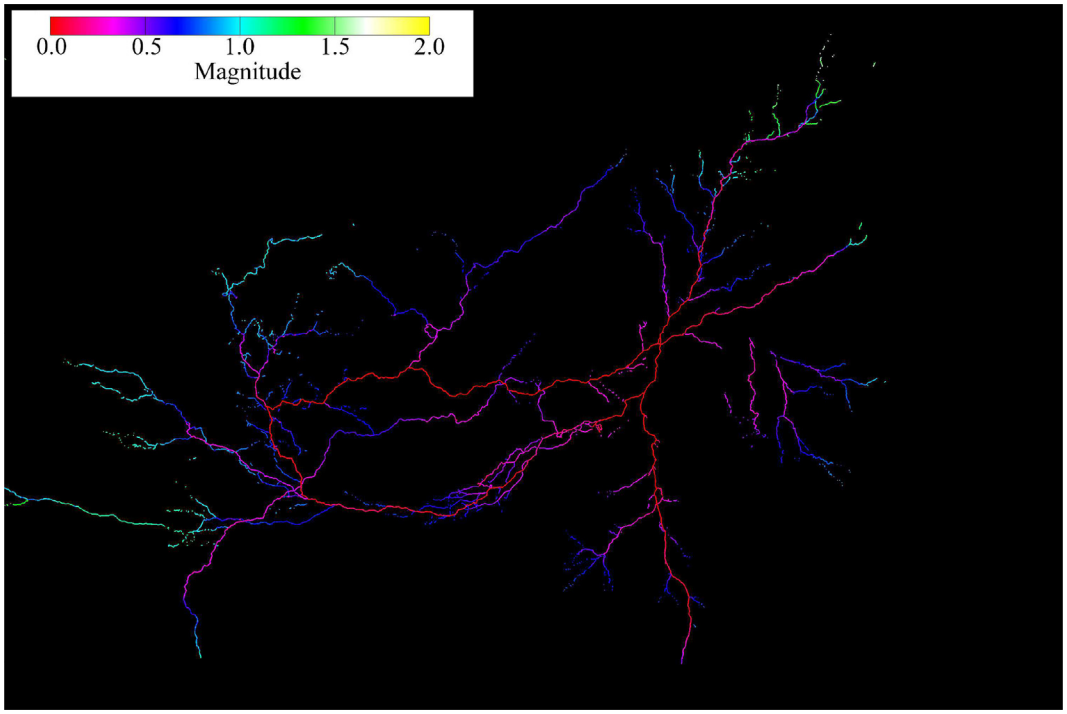

Fig. 4. 2D magnitude image of the lightning channels and branches. The image processing such as thickening does not performed to improve visibility. The scale bar ranging from 0.0 to 2.0 indicates the magnitude. (Since this figure is colored, the reader is referred to the online version article.)

That is, the pixel having the brightest value 255 is zeroth magnitude, $m_{\mathrm{ref}} = 0$. Thus from Eq. (4) we define that the apparent magnitude m for lightning leaders is given by $m_i - m_{\mathrm{ref}} = -2.5\log_{10} V_i/V_{\mathrm{ref}}$,and thus since $m_{\mathrm{ref}} = 0$,

$$m_i = -2.5\log_{10}\frac{V_i}{V_{\mathrm{ref}}}, \tag{5}$$

where V_i is the ith pixel value (in 256 levels) and V_{ref} is the reference brightness value, which is the maximum grayscale pixel value, 255 (i.e. $V_{\mathrm{ref}} = 255$).

Conversion to magnitude at equal distance

Magnitude of an object can be converted depending on the observation distance. Suppose m_1 is magnitude of an object at distances r_1, and similarly m_2 is magnitude of the same object at distance r_2. From traditional photometry, the illuminance in $\mathrm{lm}\cdot\mathrm{m}^{-2}$ is defined by $E = I/r^2$ (called inverse square law) where I is the luminant intensity in $\mathrm{lm}\cdot\mathrm{sr}^{-1}$. Y_i on an ith pixel in $\mathrm{lm}\cdot\mathrm{m}^{-2}$ is the illuminance on the pixel; thus $Y_i \propto r^{-1}$. The difference $m_1 - m_2$ is expressed as

$$\begin{aligned} m_1 - m_2 &= -2.5\log_{10}(Y_1/Y_2) \\ &= -2.5\log_{10}(r_2/r_1)^2. \\ &= -5\log_{10}(r_2/r_1). \end{aligned}$$

When magnitude m_1 at r_1 is known, m_2 at r_2 is given by

$$m_2 = m_1 - 5\log_{10}(r_1/r_2). \tag{6}$$

Results and discussion

Fig. 3 (Upper) shows the extracted lightning channels and branches. It is found that the background of the image were removed successfully. Fig. 3 (Lower) is the grayscale image

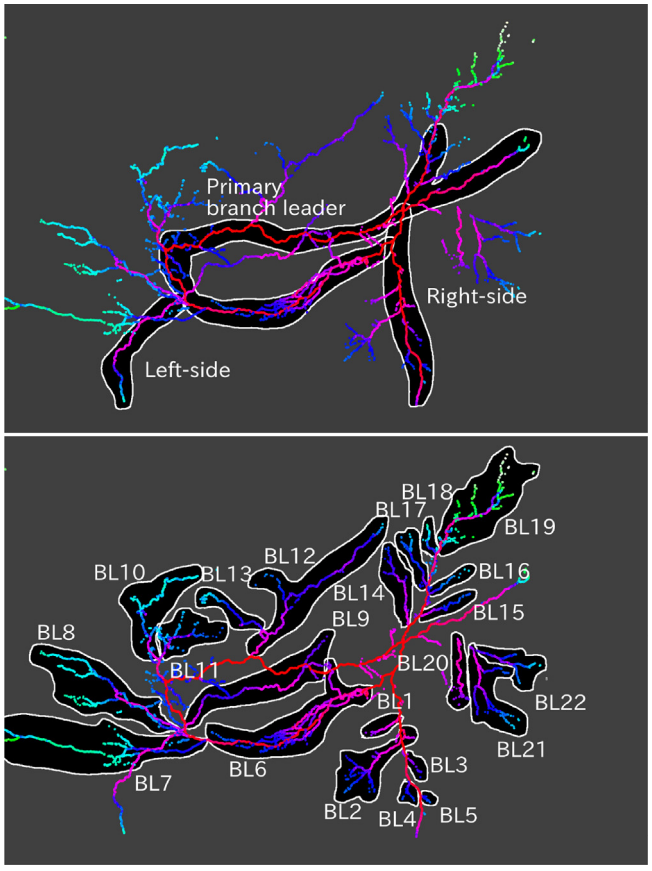

Fig. 5. (Upper) Left- and right-side strike channels and primary branched leader and (Lower) branched leaders BL1–BL22.

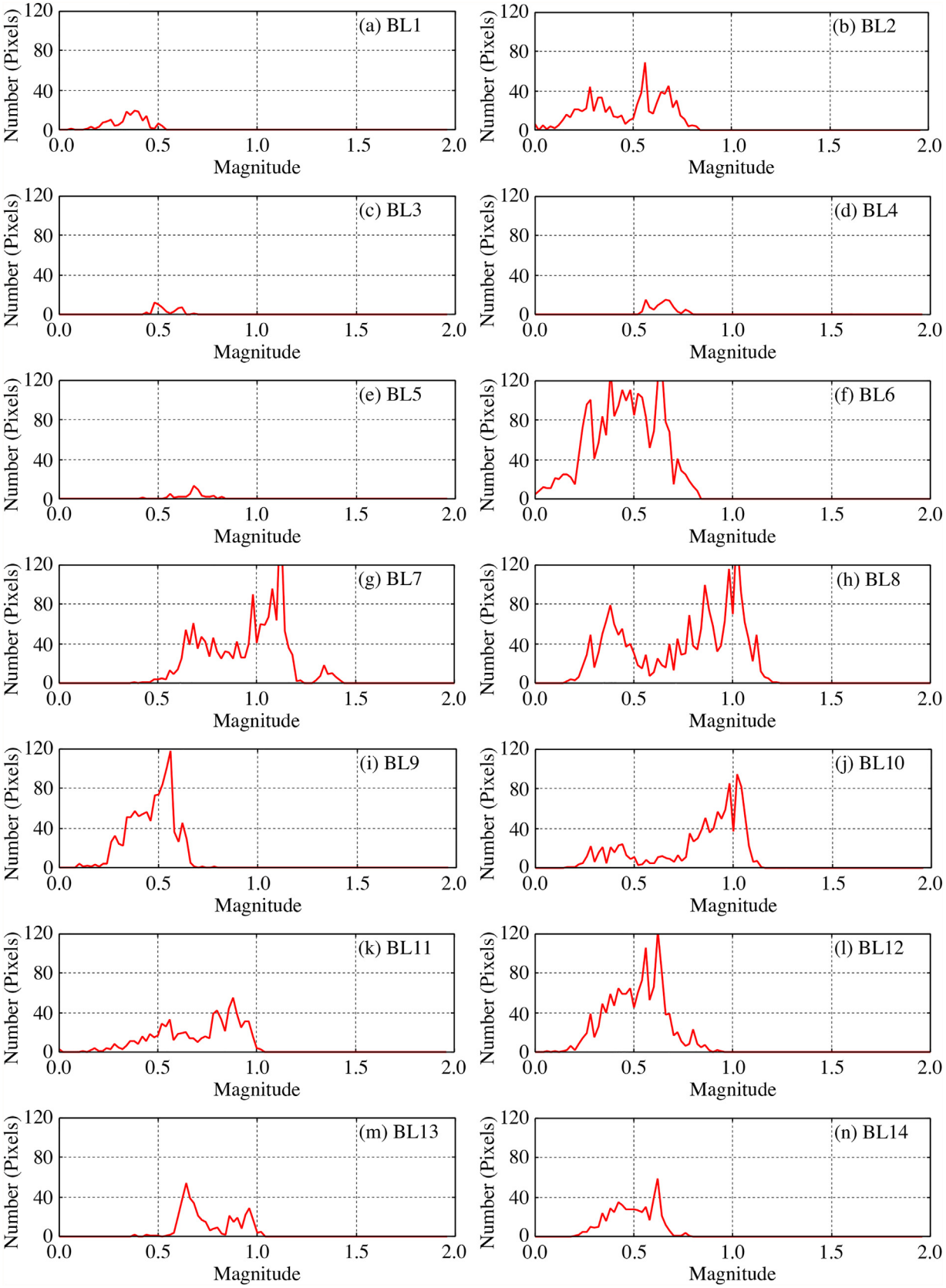

Fig. 6. Histograms of the magnitude for the channels and branched leaders in Fig. 5.

converted from Fig. 3 (Upper). At first glance, it seems that both the images Fig. 3 (Upper) and (Lower) are close to the same; however, Fig. 3 (Upper) is the RGB color image, and Fig. 3 (Lower) is the grayscale image. We used the grayscale image (Fig. 3(Lower)) to calculate the magnitude of the lightning channels and branches.

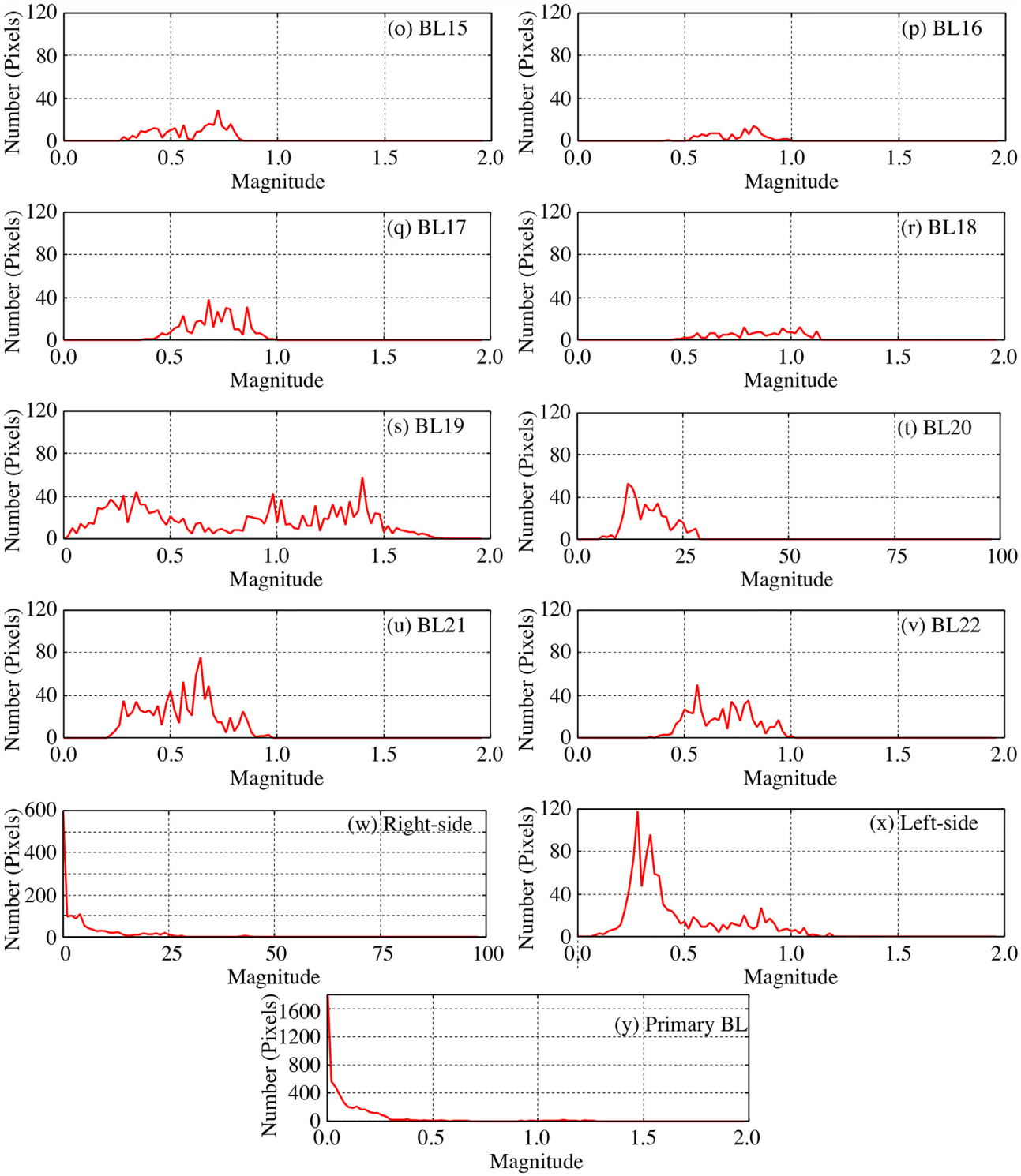

Fig. 6 (*continued*)

Fig. 4 shows the 2D magnitude image of the lightning channels and branches and it was obtained by applying Eq. (5) to Fig. 3 (Lower). It should be noticed that magnitude increases with decreasing the brightness of an object. From the assumption explained in Section "Calculation of magnitude of lightning leaders", the brightest lightning channels are zeroth magnitude. The left- and right-side strike channels, primary branched leader (primary BL) and branched leaders (BL1–BL22) are indicated in Fig. 5. The primary BL and branches BL1–BL5 are branches originated from the right-side strike channel. The left-side strike channel and branches BL6–BL19 are branches originated from the primary BL. The BL20–BL22 are emerging from the cloud and perhaps these are originated from one leader in the cloud. Furthermore, we obtained the histogram of the channels and branches in Fig. 5 (see Fig. 6). From Figs. 4 and 6, the left- and right-side strike channels, the primary BL and the branch leaders (BL1–BL22) have the following properties: the right-side strike channel and the primary BL are about zeroth magnitude (i.e. very bright)

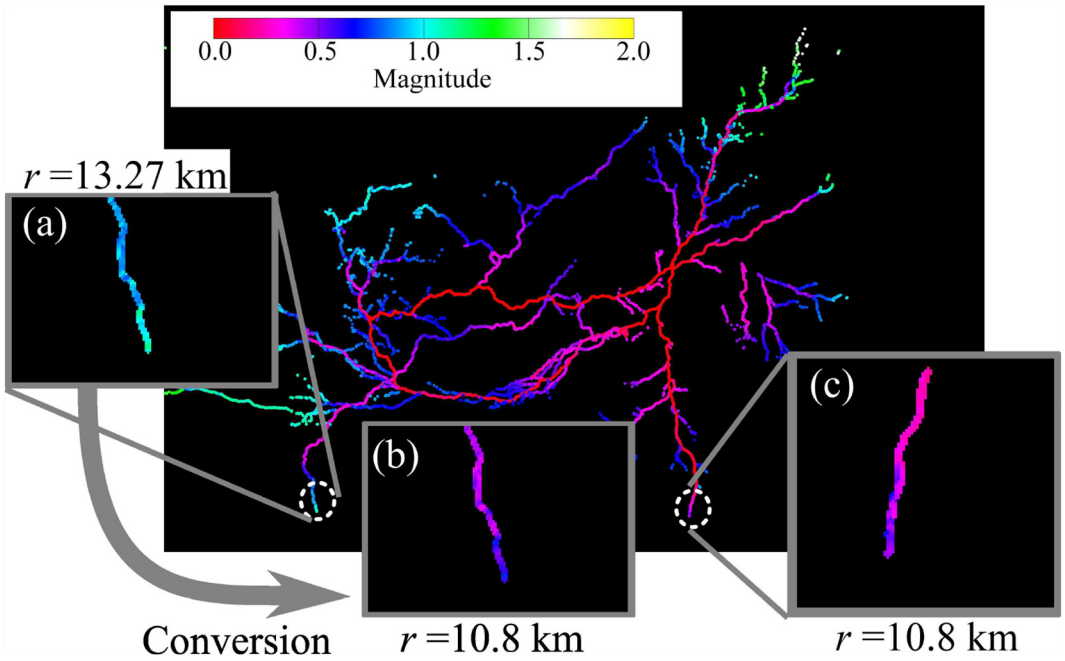

Fig. 7. Enlarged 2D magnitude images of the lower portion for (a) the left-side, (b) converted left-side and (c) right-side strike channels. (Since this figure is colored, the reader is referred to the online version article.)

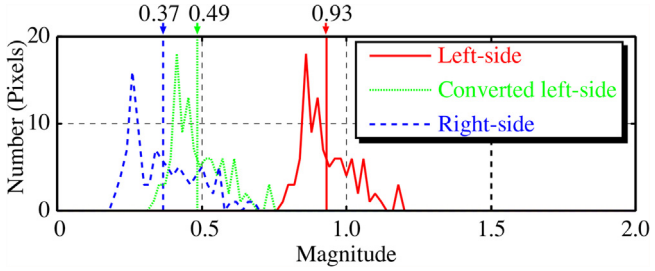

Fig. 8. Histogram of the magnitude of the lower portions for the left-side (solid line), converted left-side (dotted line) and right-side (dashed line) strike channels. The vertical lines indicate the mean value of the magnitude for the left-side (solid line), converted left-side (dotted line) and right-side (dashed line) channels. The mean values for the left-side, converted left-side and right-side strike channels are 0.93, 0.49 and 0.37, respectively.

and the left-side strike channel is about 0.25–1.0; at the tip of the branch leaders BL1–BL22, the magnitude m is relatively higher (i.e. faint); and the magnitude of the leaders gradually increases as approaching the tip of the leaders. In particular, at the tips of the branches, BL7, BL8, BL10, BL11, BL13, BL18 and BL19, the magnitude is greater than 1.0 (i.e. faint). The variation of the branch leader magnitude is the relative variation for the maximum grayscale pixel value 255 (in 256 levels). As seen above, it was found from Figs. 4 and 6 that the branch leader magnitude vary spatially.

We have investigated the magnitude of the left- and right- side strike channel at equal distance. The left- and right-side strike points were identified as explained in Appendix B and it was found that the distance r_{left} between the camera and left-side strike point is 13.27 km, and similarly $r_{\text{right}} = 10.8$ km. Using the Eq. (6), we converted the magnitude m_{left} of the left-side strike channel at the distance $r_{\text{left}} = 13.27$ km to the magnitude m'_{left} at the distance $r'_{\text{left}} = 10.8$ km ($= r_{\text{right}}$); and this can be expressed as follows:

$$m'_{\text{left}} = m_{\text{left}} - 5\log_{10}(r_{\text{left}}/r_{\text{right}}) = m_{\text{left}} - 5\log_{10}(13.27/10.8).$$

In conversion, we restricted to the lower portions of the left- and right-side strike channels, since the lower portion of the right-side strike channel is unsaturated to 255 (in 256 levels). In Fig. 7 the enlarged figures of the lower portions for the left-side, converted left side and right-side channels are denoted. From Fig. 7 (b) and (c), the magnitude of the lower portion of the left-side strike channel is close to that of the right-side, at the equal distance ($r'_{\text{left}} = r_{\text{right}} = 10.8$ km). Fig. 8 is the histogram of the magnitude m_{left} and m_{right} for the left- and right-side strike channels and the converted magnitude m'_{left} of the left-side strike channel. The mean values of the magnitude m_{left} and the converted magnitude m'_{left} for the left-side strike channel and the magnitude m_{right} for the right-side strike channel are obtained as: $\langle m_{\text{left}}\rangle = 0.93, \langle m'_{\text{left}}\rangle = 0.49$ and $\langle m_{\text{right}}\rangle = 0.37$. It can be seen that the converted magnitude m'_{left} of the left-side strike channel decreased. The absolute difference between the mean values $\langle m_{\text{right}}\rangle$ and $\langle m'_{\text{left}}\rangle$ is 0.12. The absolute difference $|\langle m_{\text{right}}\rangle - \langle m'_{\text{left}}\rangle|$ means that in the case of the equal distance ($r'_{\text{left}} = r_{\text{right}} = 10.8$ km the magnitude of the right-side strike channel is 0.12 lower than that of the left-side strike channel. As explained in Section "Material and calculation method" and Appendix B, the peak currents of the left- and right-side strike channels are $I_{\text{left}} = 11$ kA and $I_{\text{right}} = 35$ kA, (i.e. $I_{\text{left}} < I_{\text{right}}$). Therefore, we can infer that the high current channel is low magnitude (i.e. bright) and the low current channel is high magnitude (i.e. faint). This inference coincide with the relation between the channel brightness and channel current (hereinafter called brightness – current relation) reported in Refs. [2–6] in which it has been described that the channel brightness increases with increasing the channel current. Since in this paper, we evaluate the leader brightness by the leader magnitude, the brightness–current relation can be rewritten as the relation between the channel magnitude and channel current (hereinafter called magnitude–current relation).

In Ref. [20], it is reported that the correlated color temperature (CCT), T^{CCT}, of the high current channel (i.e. right-side strike channel) is higher than that of the low current channel (i.e. left-side strike channel); that is, $T^{\text{CCT}}_{\text{left}} < T^{\text{CCT}}_{\text{right}}$ and $I_{\text{left}} < I_{\text{right}}$. It should be noted that the CCT is different to the actual temperature. From

Table A.1
Specification of the digital still camera (Canon EOS KISS Digital X).

Image sensor	High-sensitivity, high-resolution, Large, single-plate CMOS sensor
Sensor size	22.2 × 14.8 mm
Effective pixels	approximately 10.1 megapixels: 3904 (H) × 2598 (V) pixels
Total pixels	approximately 10.5 megapixels: 3996 (H) × 2622 (V) pixels
Pixel unit	5.7 μm square
Aspect ratio	2: 3 (Vertical: Horizontal)
Color filter type	RGB primary color filters
Low-pass filter	Fixed position in front of the image sensor
Image engine	DIGIC II
RAW quality	lossless RAW and 12 bit digital output (The extension for RAW images is CR2.)

the results ($m_{right} < m_{left}$ and $I_{left} < I_{right}$) in this study and ($T^{CCT}_{left} < T^{CCT}_{right}$ and $I_{left} < I_{right}$) in the previous study [20], we can speculate that the channel magnitude is correlated with both the channel current I and the CCT T^{CCT} of lightning channel.

In this study, the relative magnitude variation for the reference brightness, which is maximum grayscale pixel value $V_{ref} = 255$ (in 256 levels) was confirmed. In astronomy, the research investigating light emitted from stars has made major advances by defining standard reference stars. For this reason, it is necessary to define the standard reference source for the lightning research.

In astronomical photometry, there are two methods: differential photometry and absolute photometry. The differential photometry defines the relative brightness of a star comparing with other star. Brightness evaluation of lightning leaders discussed in this work is the same with the differential photometry in astronomical photometry. If the absolute photometry for the brightness of lightning leader is developed, the comparisons between different images showing lightning flash are possible. Furthermore, the comparability between the magnitude of the brightness for lightning channels and branches and other observations such as channel current and electric field, must be investigated in future research.

It can be considered that the magnitude system can apply to high-speed digital video image. Recently, the lightning researches using the high-speed digital video camera have been reported (for example, Refs. [21–25]). If the magnitude system is applied to high-speed video data, the spatio-temporal variability of lightning channel will be obtained. Furthermore, in upper atmospheric physics, the many researches for the transient luminous event is reported (for example Refs. [26–29]). We consider that the magnitude system can also be applied to analyze the upper-atmospheric discharge such as sprite, elvse and blue-jets.

Conclusions

In this study, it was found that the brightness of lightning channels and branches can be evaluated quantitatively by using the magnitude system. The channel and branch magnitude suggested spatial variability. Moreover, comparing the channel magnitude and the channel currents we obtained the result that the high current channel is the low magnitude and the low current channel is the high magnitude. Furthermore, the magnitude–current relation obtained in this work coincided with the brightness–current relation reported in Refs. [2–6]. For this reason, it was found that the magnitude system can be applied to quantitatively evaluate the brightness of lightning channel and branche.

Acknowledgments

We would like to thank Mr. Yutaka Aoki, a free nature photographer specializing in severe weather events, for providing the digital still image of lightning flash and Franklin Japan Corporation for providing the JLDN data. We used Google earth™ for investigation of the geographical location of the lightning events. We are grateful to Mr. Shingo Sakihama, Mr. Ryoma Aoyama, Mr. Wataru Hasegawa and Mr. Yamato Uehara for valuable discussion and assistance in several calculation and anonymous reviewer(s) for useful comments.

Appendix A. Specification of the digital camera

The specification of the digital camera used in this work is shown in Table A.1.[6]

Appendix B. Identification of the lightning events in the lightning flash image

We have identified the strike points in the lightning image (Fig. 2) using the lightning data in Table B.1. The data in Table B.1 denote the lightning events in 21:15–22:15 JST (12:15–13:15 UTC) in the investigation area in Chikusei City, Ibaraki Prefecture, Japan, on October 27th, 2008. The investigation area is 15 km × 15 km and the center of the investigation area is located at lat. 36.350173°N (DD) and long. 140.045198°E (DD). The detection efficiency of the JLDN is greater than 90% for CG flashes and 40% for IC flashes; the median location accuracy of the JLDN is better than 0.5 km.[7] The data in Table B.1 include ID numbers, time JST, the location (lat. and long.), the polarity (+/−), the estimated peak current (kA), and CG/IC index. The time in Table B.1 is based on the JST.

We have investigated the geographic locations of the left- and right-side strike points in Fig. 2 using the lightning event data in Table B.1. Fig. B.1 shows the locations of the lightning events in Table B.1 and the photographing location. In Fig. B.1, there are some candidates of the left- and right-side strike points in the lightning image (Fig. 2) along the two long straight-lines in Fig. B.1. Therefore it is difficult to identify the lightning strike points by means of the only geographical location.

We have depicted the schematic illustration (Fig. B.2) of the time with respect to the lightning events in Table B.1 and the exposure duration for the lightning image (Fig. 2). Fig. B.2(a) shows the individual times of the IC flash events in Table B.1; and it is found that there are 9 IC flash events in 21:15–22:15 JST (12:15–13:15 UTC). Fig. B.2(b) shows the individual times of the CG flash events in Table B.1. In Fig. B.2(b), there are twenty-one lightning events in 21:15–22:15 JST (12: 15–13:15 UTC), while it seems that there are fourteen lightning events. Namely, seven CG flash events are overlapping since these events occurred nearly simultaneously. In Fig. B.2(b), the approximately simultaneous events are indicated by the dashed lines. Fig. B.2(c) shows the exposure duration for the lightning image in Fig. 2. By comparing Fig. B.2(b) and (c), it follows that the lightning events, ID: 20 and ID: 21, are most appro-

[6] The specification of the camera are explained in the instruction manual (in Japanese) and service manual (in English) for Canon EOS Kiss Digital X.

[7] The details for the JLDN is explained in the JLDN technical description (in Japanese).

Table B.1
Lightning data in 21:15–22:15 JST (12:15–13:15 UTC) in the investigation area in Chikusei City, Ibaraki Prefecture, Japan, on October 27th, 2008. The data is provided by Franklin Japan Corporation. The latitude and longitude are given in decimal degrees (DD).

ID	Time JST	Lightning location (WGS 84)		Polarity	Peak current	CG/IC
	(ns)	Latitude (DD)	Longitude (DD)	+/−	(kA)	
1	21:17:6:591327450	36.3683°N	139.9669°E	−	6	CG
2	21:18:27:558320409	36.3536°N	139.9745°E	−	13	IC
3	21:18:27:589571036	36.3428°N	139.9891°E	−	28	CG
4	21:18:27:735903133	36.328°N	139.9989°E	−	9	CG
5	21:20:40:116117691	36.3649°N	139.9905°E	−	68	CG
6	21:20:40:148843700	36.3569°N	139.9951°E	−	12	CG
7	21:21:19:214825550	36.3473°N	139.978°E	+	7	CG
8	21:22:12:826584983	36.3561°N	139.9834°E	−	31	CG
9	21:22:12:849340650	36.3965°N	140.0426°E	−	13	CG
10	21:23:2:212293887	36.334°N	140.0356°E	+	14	CG
11	21:23:58:705277763	36.3595°N	140.0087°E	−	11	CG
12	21:24:10:326889443	36.3608°N	139.98°E	+	8	IC
13	21:25:18:83780450	36.3327°N	140.052°E	−	15	CG
14	21:25:18:83784281	36.3583°N	140.0108°E	−	21	CG
15	21:25:18:108304626	36.3747°N	139.9733°E	−	6	CG
16	21:25:39:614264250	36.3662°N	139.9693°E	+	7	IC
17	21:28:9:397386500	36.3708°N	139.9782°E	−	19	IC
18	21:28:9:418860575	36.3836°N	140.077°E	−	5	CG
19	21:29:41:912989800	36.3322°N	139.9863°E	+	5	IC
20	21:32:15:530283215	36.316°N	140.0776°E	−	35	CG
21	21:32:15:603968541	36.376°N	140.0589°E	−	11	CG
22	21:33:12:666414500	36.3266°N	140.0708°E	+	14	CG
23	21:33:12:667979150	36.3639°N	140.032°E	+	7	IC
24	21:34:0:937847200	36.3565°N	140.0204°E	+	11	IC
25	21:41:58:745186600	36.3424°N	140.0718°E	+	8	CG
26	21:44:16:176844671	36.338°N	140.0767°E	−	43	CG
27	21:44:16:187369400	36.3374°N	140.1224°E	−	7	CG
28	21:46:29:646441950	36.3721°N	140.0536°E	+	5	IC
29	21:46:29:847440271	36.4008°N	140.0779°E	+	31	CG
30	22:3:21:489762200	36.3375°N	140.1234°E	−	7	IC

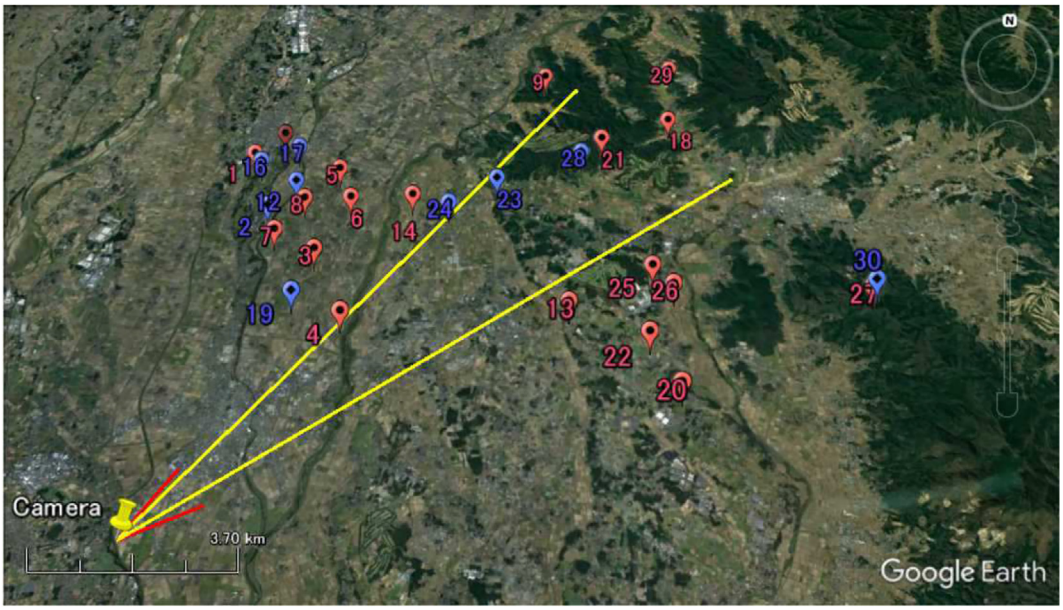

Fig. B.1. Locations of the lightning events in Table B.1. The location of the CG events is marked with the balloon icon in which the symbol, solid circle is written; similarly that of the IC events is marked with the balloon icon in which the symbol, solid diamond is written. The number attached to the balloon icons is the ID number in Table B.1. The camera location is marked as the pushpin icon. The two short solid lines near the camera denote the field of view of Fig. 2. The two long straight-lines denote the approximate directions of the strike points shown in Fig. 2. The scale bar in the bottom left corner indicates the range 0–3.70 km. (Image courtesy of Google earth™.)

priate to the CG flash events in Fig. 2. Thus we determined that the lightning event of the ID: 20 is the right-side strike point in Fig. 2. Similarly the lightning event of the ID: 21 is the left-side strike point in Fig. 2. From Table B.1, the peak currents of the events, ID: 20 and ID: 21, are 35 kA and 11 kA, i.e. $I_{\text{left}} = 11$ kA and $I_{\text{right}} = 35$ kA.

Appendix C. Details of Extraction of lightning leaders

Fig. C.1 shows the image processing flowchart for extracting lightning leaders. It is seen from Fig. C.1 that the extraction method is based on masking. This is simple, however creating a precise mask image is difficult.

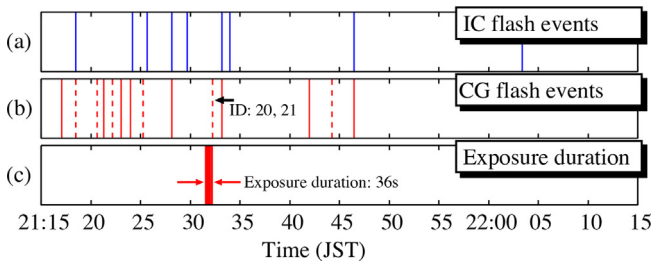

Fig. B.2. Schematic illustration of the time JST for the (a) IC and (b) CG flash events shown in Table B.1 and for (c) the exposure duration of Fig. 2. The solid lines in (b) indicate the single event; and the dashed lines in (b) indicate the approximately simultaneous events occurred within one second. The beginning time of the exposure for the lightning image (Fig. 2) is 21:31:33 JST (12:31:33 UTC). The exposure duration for the lightning image (Fig. 2) is 36 s.

The process (b)–(f) in Fig. C.1 is to obtain the mask image in which bright leaders are extracted well; however, the extraction of faint leaders are incomplete. The image (g) is the mask image for the bright leaders. For the process (h)–(m), we also created the mask image that clearly shows the faint leaders, however it is incomplete for the bright leaders. The image (n) is the mask image for the faint leaders. Merging the mask images (g) and (n) at the step (o), the complete mask image (p) was obtained. Masking at the step (q) yields the extracted mask image (r).

The details of each step in Fig. C.1 are explained in the following.

(a) Original image. The original image is shown in Fig. 2.

(b) Thresholding. The threshold operator is expressed as

$$dst(x,y) = \begin{cases} 255 & \text{if } src(x,y) > \text{threshold value}, \\ 0 & \text{if } src(x,y) \leqslant \text{threshold value}, \end{cases}$$

where $src(x,y)$ is the (x,y) component of an input image and $dst(x,y)$ is the (x,y) component of an output binary image. We used the function "cvThreshold" in OpenCV library to perform thresholding and set "CV_THRESH_BINARY" to the parameter of the function. We performed the thresholding in parallel changing the threshold values 63, 65, 70, 75, 80, 85, 90, 95, 100, 105, 120, 135, 150, 170, 200, 220 in 256 levels. Thus 16 images were obtained in the step (b).

(c) Manual correction. In the thresholding images obtained in the previous step (b), there are many unwanted parts such as artificial light and cloud luminescence. These were removed carefully and manually in the step (c). Since 16 images were obtained in the step (b), the manual correction in the step (c) are performed in parallel.

(d) Thinning. We adopted the Zhang-Shuen thinning algorithm [30] for the thinning. Since there is no the Zhang-Suen thinning algorithm in the OpenCV library, we made the program code for the Zhang-Suen algorithm. The thinning algorithm is applied in parallel to the 16 images obtained in the previous step (c).

(e) Pixel addition. In the step (e), we merged the 16 images obtained in the step (d).

(f) Manual correction. In this step fine noises were removed by repeating manual-handling task and visual check.

(g) Mask image clearly showing bright leaders. Performing the steps from (b) to (f) yields the mask image clearly showing the bright leaders.

The mask image clearly showing faint leaders was created through the following steps (h)–(m):

(h) Sobel edge detection. We performed the sobel edge detector to the original image (Fig. 2). The sobel edge detector uses the two convolution kernels H_x in the x direction and H_y in the y direction shown as:

$$H_x = \begin{bmatrix} -1 & 0 & 1 \\ -2 & 0 & 2 \\ -1 & 0 & 1 \end{bmatrix}, \quad H_y = \begin{bmatrix} -1 & -2 & -1 \\ 0 & 0 & 0 \\ 1 & 2 & 1 \end{bmatrix}.$$

We used the function "cvSobel" in OpenCV library. Computation was performed by setting "1" as the order of the derivative x and y directions and "3" as the kernel size. Applying the sobel operator to the original image (Fig. 2) yields an edge detection image, which is a grayscale image.

(i) Thresholding. We used the function "cvThreshold" in OpenCV library as with the step (b). The threshold value was set to "15" in 256 levels.

(j) Manual correction. It was confirmed that in the thresholding image obtained in the step (i), there are many unwanted parts caused by the artificial light and cloud luminescence shown in the original image (Fig. 2). These were removed carefully and manually by repeating manual-handling task and visual check.

(k) Thickening. In the images obtained in the step (j), there are lacking parts in lightning channels look like holes. Thus we filled the holes by performing thickening. We performed the thickening by applying a function "cvDilate" in OpenCV library to the image obtained in the previous step (j); and a parameter "iterations" was set to "1".

(l) Thinning. We adopted the Zhang-Shuen thinning algorithm [30] for the thinning as with the step (d).

Applying steps (h)–(m) to the original image yields the mask image (n) clearly showing the faint leaders.

(o) Pixel addition and (p) Complete mask image. The mask images (g) and (n) were merged in the step (o) and then the complete mask image (p) was obtained.

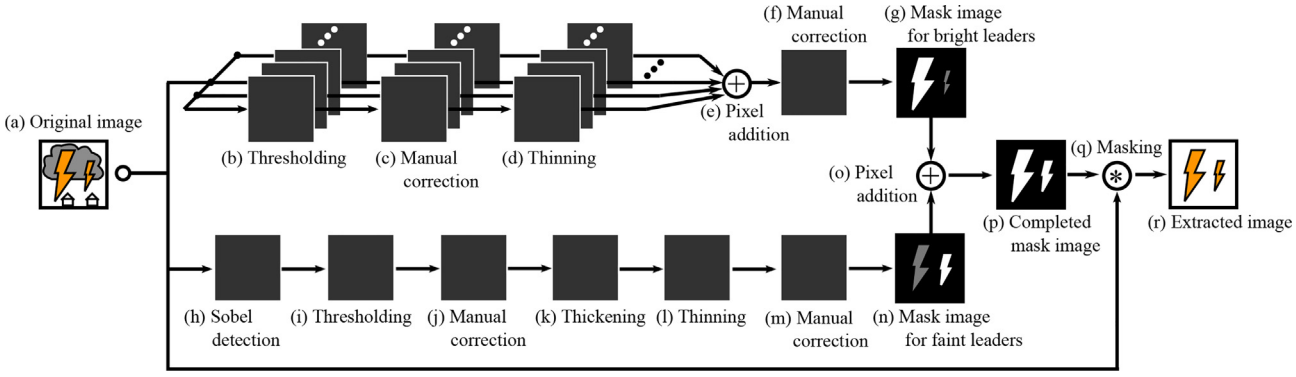

Fig. C.1. Image processing flowchart for extracting lightning leaders shown in a digital still image.

(q) Masking and (r) Extracted image. In the step (q) masking was performed and the extracted image (r) was obtained.

References

[1] Flowers JW. The channel of the spark discharge. Phys Rev 1943;64:225–35. http://dx.doi.org/10.1103/PhysRev. 64.225.

[2] Idone VP, Orville RE. Correlated peak relative light intensity and peak current in triggered lightning subsequent return strokes. J Geophys Res 1985;90:6159–64. http://dx.doi.org/10.1029/JD090iD04p06159.

[3] Gomes C, Cooray V. Correlation between the optical signatures and current wave forms of long sparks: applications in lightning research. J Electrostat 1998;43:267–74. http://dx.doi.org/10.1016/S0304-3886(98)00008-4.

[4] Wang D, Takagi N, Watanabe T, Rakov VA, Uman MA, Rambo KJ, et al. A comparison of channel-base currents and optical signals for rocket-triggered lightning strokes. Atmos Res 2005;76:412–22. http://dx.doi.org/10.1016/j.atmosres.2004.11.025.

[5] Amarasinghe D, Sonnadara U, Berg M, Cooray V. Correlation between brightness and channel currents of electrical discharges. IEEE Trans Dielectr Electr Insul 2007;14:1154–60. http://dx.doi.org/10.1109/TDEI.2007.4339475.

[6] Zhou E, Lu W, Zhang Y, Zhu B, Zheng D, Zhang Y. Correlation analysis between the channel current and luminosity of initial continuous and continuing current processes in an artificially triggered lightning flash. Atmos Res 2013;129–130:79–89. http://dx.doi.org/10.1016/j.atmosres.2012.10.020.

[7] Schaaf Fred. The brightest stars: discovering the universe through the sky's most brilliant stars. 1st ed. New Jersey, USA: John Wiley and Sons, Inc.; 2008. ISBN(13): 9780471704102.

[8] Seeds MA, Backman D. Stars and galaxies. 8th ed. Connecticut, USA: Cengage Learning; 2012. ISBN(13): 978-1111990664.

[9] Jones D. Norman Pogson and the definition of stellar magnitude. Astr Soc Pacific Leafl 1967;10:145–52. Bibliographic Code: 1968ASPL10.145J.

[10] Pliskoff SS. Antecedent's to fechner's law: the astronomers J. Herschel, W.R. Dawes, and N.R. Pogson. J Exp Anal Behav 1977;28:185–7. http://dx.doi.org/10.1901/jeab.1977.28-185.

[11] Webb S. Measuring the universe: the cosmological distance ladder, 1999th edition, Springer praxis space exploration. London, UK: Springer-Verlag; 2008. ISBN(13): 978-1852331061.

[12] Brown BH, Smallwood RH, Barber DC, Lawford PV, Hose DR. Medical physics and biomedical engineering, medical science series. Bristol, UK and Philadelphia, USA: Institute of Physics Publishing; 1999. ISBN(13): 978-0750303682.

[13] Orville RE, Uman MA. The optical continuum of lightning. J Geophys Res 1965;70:279–82. http://dx.doi.org/10.1029/JZ070i002p00279.

[14] Uman MA, Orville RE. The opacity of lightning. J Geophys Res 1965;70:5491–7. http://dx.doi.org/10.1029/JZ070i022p05491.

[15] Reinhard E, Ward G, Pattanaik S, Debevec P, Heidrich W, Myszkowski K. High dynamic range imaging: acquisition, display, and image-based lighting. Burlington, Massachusetts, USA: Morgan Kaufmann; 2010. ISBN (13): 978-0123749147.

[16] Burger W, Burge MJ. Digital image processing: an algorithmic introduction using Java. New York: Springer-Verlag; 2008. http://dx.doi.org/10.1007/978-1-84628-968-2.

[17] International Telecommunication Union. Recommendation ITU-R BT.709-5 (04/2002). Parameter values for the HDTV standards for production and international programme exchange, https://www.itu.int/rec/R-REC-BT.709-5-200204-S/en, (downloaded on December 26, 2016).

[18] Schanda J. Colorimetry: understanding the CIE system. 1st ed. New Jersey, USA: Wiley-Interscience; 2007. http://dx.doi.org/10.1002/9780470175637.

[19] Bradski G, Kaehler A. Learning OpenCV: computer vision with the OpenCV library. 1st ed. USA: O'Reilly Media; 2008. ISBN(13): 978-0596516130.

[20] Shimoji N, Aoyama R, Hasegawa W. Spatial variability of correlated color temperature of lightning channels. Res Phys 2016;6:161–2. http://dx.doi.org/10.1016/j.rinp.2016.03.004.

[21] Warner Tom A. Observations of simultaneous upward lightning leaders from multiple tall structures. Atmos Res 2012;117:45–54. http://dx.doi.org/10.1016/j.atmosres.2011.07.004.

[22] Mazur V, Ruhnke LH, Warner TA, Orville RE. Recoil leader formation and development. J Electrostat 2013;71:763–8. http://dx.doi.org/10.1016/j.elstat.2013.05.001.

[23] Campos LZS, Saba MMF, Warner TA, Pinto Jr O, Krider EP, Orville RE. High-speed video observations of natural cloud-to-ground lightning leaders – a statistical analysis. Atmos Res 2014;135–136:285–305. http://dx.doi.org/10.1016/j.atmosres.2012.12.011.

[24] Saba MMF, Schumann C, Warner TA, Helsdon JH, Orville RE. High-speed video and electric field observation of a negative upward leader connecting a downward positive leader in a positive cloud-to-ground flash. Electr Power Syst Res 2015;118:89–92. http://dx.doi.org/10.1016/j.epsr.2014.06.002.

[25] Qi Q, Lu W, Ma Y, Chen L, Zhang Y, Rakov VA. High-speed video observations of the fine structure of a natural negative stepped leader at close distance. Atmos Res 2016;178–179:260–7. http://dx.doi.org/10.1016/j.atmosres.2016.03.027.

[26] Boeck WL, Vaughan Jr OH, Blakeslee RJ, Vonnegut B, Brook M. The role of the space shuttle videotapes in the discovery of sprites, jets and elves. J Atmos Sol Terr Phys 1998;60:669–77. http://dx.doi.org/10.1016/S1364-6826(98)00025-X.

[27] Chern RJS, Lin S, Wu A. Ten-year transient luminous events and Earth observations of FORMOSAT-2. Acta Astronaut 2015;112:37–47. http://dx.doi.org/10.1016/j.actaastro.2015.02.030.

[28] Siingh D, Singh RP, Kumar S, Dharmaraj T, Singh AK, Singh AK, et al. Lightning and middle atmospheric discharges in the atmosphere. J Atmos Sol Terr Phys 2015;134:78–101. http://dx.doi.org/10.1016/j.jastp.2015.10.001.

[29] Liu N, McHarg MG, Stenbaek-Nielsen HC. High-altitude electrical discharges associated with thunderstorms and lightning. J Atmos Sol Terr Phys 2015;13:98–118. http://dx.doi.org/10.1016/j.jastp.2015.05.013.

[30] Zhang TY, Suen CY. A fast parallel algorithm for thinning digital patterns. Commun ACM 1984;27:236–9. http://dx.doi.org/10.1145/357994.358023.